

Giant Rashba electrical control of magnetism in band models

Wen Li and Stewart Barnes

Physics Department, University of Miami, Coral Gables, 33124,
FL, USA.

*Corresponding author(s). E-mail(s): wxl386@miami.edu;
sbarnes@miami.edu;

Abstract

It is of considerable technological importance to achieve an electrical control of magnetism of sufficient magnitude. To overcome the in-plane shape anisotropy, needed is the electrical control of a perpendicular magnetic anisotropy (PMA). It is known, within a free electron model, the Rashba spin-orbit coupling provides such a control. Surprisingly, this same Rashba PMA is enhanced by two to three orders of magnitude when a periodic potential is added. Usually spin Berry phase physics reflects time dependent magnetic fields. Here it is shown, within a time independent model, such physics arises because the Rashba effective magnetic field has texture within the unit cell. Predicted are electrical controllable band-structure gaps, linear in the applied electric field \mathbf{E} , that can result in a truly giant linear PMA. Also possible is a Peierls mechanism, in which the magnetisation tilts from the vertical, shifting these gaps to the Fermi level. As a consequence there are low dissipation electric field driven dynamics, an alternative to the more dissipative spin torque transfer (STT) effect. The theory requires the introduction of an intrinsic spin Berry connection $\vec{\mathbf{A}}_s$, an effective vector potential, and is incompatible with current density functional theories (DFT).

For magnetic memory applications, it is estimated[1], an electrical control of magnetism coefficient of $\gtrsim 200$ fJ/Vm is needed. This remains an elusive goal. Here the more modest aim is to find an effective Rashba magnetic field \vec{B}_R of magnitude $\sim 1 - 10$ T. Within the free electron model, Barnes et al[2] have shown the Rashba spin-orbit-coupling can generate the necessary PMA,

proportional to E^2 , but for two dimensions, there are two contributions to the magnetic anisotropy that almost cancel. This near cancellation no longer occurs when a periodic potential $V(\vec{r})$ is accounted for. The PMA contribution dominates leading to a massive increase in this anisotropy energy. In addition, for a (near) perpendicular magnetisation \vec{M} , the periodic potential introduces spin Berry phase physics described by a connection \vec{A}_s proposed some time ago [3]. Even in one dimension, as an electron is repeatedly reflected, it precesses on the Bloch spin sphere. The resulting spin mixing opens electrically controlled band structure gaps, linear in E , near points at which there is an accidental degeneracy of the majority/minority bands. For suitable material parameters, implied is a truly giant PMA. A Peierls effect[4, 5] is another consequence of this spin Berry phase physics. The magnetisation \vec{M} tilts away from the vertical thereby shifting the spin gaps to the Fermi level. Implied, in addition to a giant PMA, are electric field driven dynamics, an alternative to the more dissipative spin torque transfer (STT) effect[3, 6].

Kept in mind, as an illustrative example, are ultra-thin magnetic layers with a PMA induced by an equally thin Au layer. There is a small exchange splitting induced by the magnetic proximity effect. The aim is to have an exchange field \vec{B}_E of a similar magnitude to the effective Rashba field \vec{B}_R .

Spin-orbit coupling. While the spin-orbit coupling is implicit in the Dirac equation[7] it appears explicitly, as $V_{so} = -\frac{e\hbar}{4m^2c^2}\vec{E} \cdot (\vec{\sigma} \times \vec{p}) = -\mu_B \frac{1}{2c^2}\vec{E} \cdot (\vec{\sigma} \times \vec{v}) = -\frac{\lambda_c}{8\pi mc}\vec{E} \cdot (\vec{\sigma} \times \vec{p})$, where $\lambda_c \approx 2\text{pm}$ is the Compton wavelength, and μ_B the Bohr magneton, only when the Dirac equation is reduced to that of Pauli using e.g., the Foldy-Wouthuysen (FW) transformation[8]. It is customary[9] to insist \vec{E} is large only in the core region where the wave-functions are atomic like and it follows[7] V_{so} reduces to the more familiar $v_{so} = \xi(r)\vec{\sigma} \cdot \vec{\ell}$ where $\xi(r) = \frac{e\hbar}{4m^2c^2} \frac{1}{r} \frac{dV_1(r)}{dr}$ and where $V_1(r)$ is the Coulomb potential of the atomic core[9, 10]. It is invariably v_{so} that is used to develop a theory of the Rashba effect[9, 11–15] and it is this that is included in the popular flavours of the DFT[16–19]. A number of methods[20], give accurate values of v_{so} and such information is included in the best DFT. However, it remains useful to estimate v_{so} [21, 22]. Following Landau and Lifshitz[21]: $\langle \xi(r) \rangle \approx \frac{1}{2} \frac{1}{n(\ell + \frac{1}{2})(\ell + 1)} (\alpha Z)^2 |E_n|$ where $E_n = -\frac{me^4}{2\hbar^2} \frac{1}{n^2}$ are the hydrogen energy eigenvalues, α is the fine-structure constant and Z the atomic number. This is consistent with the fundamental idea that the V_{so} is the second order $(\alpha Z)^2$, QED correction to the energy E_n of an outer electron. Usually[21] mixing with the core 1s-electron is accounted for by setting the principal and angular momentum quantum numbers to $n = 1$ and $\ell = 0$ resulting in $\langle \xi(r) \rangle \approx 2.6\text{eV}$ for $Z = 79$ appropriate to Au. However that $\vec{\ell}$ be finite, it is rather mixing with the core 2p-electrons with $n = 2$ and $\ell = 1$ that is appropriate. This drastically reduces $\langle \xi(r) \rangle \approx 100\text{meV}$, and is actually consistent with the Rashba splitting of the surface state of Au. A similar estimate[22, 23] for the Au electric field in the core is $\langle E \rangle \approx 1.2 \times 10^{16}\text{V/m}$ while the $\ell = 1$ tangential velocity $v \sim 0.15c$. It is hard to imagine a gating field greater than $E \sim 10^{11}\text{V/m}$ leading to Rashba field

$B_R \sim 10^{-2}\text{T}$ when corrected by the usual factor of $\frac{1}{Z^2}$ [21, 22]. Such small fields are of little technological importance. Here, it is not disputed that the DFT can accurately include v_{so} , rather it is observed that $\vec{\ell} = \vec{r} \times \vec{p}$ accounts only for the tangential component of \vec{p} while for a more or less uniform \vec{E} , due to either a surface, a lack of inversion symmetry, and/or gating, it is the entire in-plane \vec{p} that counts and account must be taken of the entire spin-orbit coupling V_{so} .

Evidently the free electron Rashba model considered by Barnes et al. [2] lacks a radial potential $V(r)$ and v_{so} is simply absent. Unfortunately the magnitude of the predicted PMA is many orders of magnitude too small to be interesting, and worse, in two dimensions a term that favours an in plane magnetisation cancels the PMA to leading order [2]. In this case the full $V_{\text{so}} = \frac{\alpha_R}{\hbar} \vec{\sigma} \cdot (\vec{p} \times \hat{\mathbf{z}})$, for $\vec{E} = \hat{\mathbf{z}}E$, constitutes the Rashba spin-orbit coupling and importantly involves the canonical momentum $\vec{p} = \hbar\vec{k}$ and not just the crystal momentum $\hbar\vec{q}$. The current exercise extends Ref. [2] by including the effects of a periodic potential in a toy Kronig-Penny model for which v_{so} remains absent. Bloch's theorem now insists, e.g., a one dimensional wave-function is a linear combination of $e^{i(q+G_n)x}$ that corresponds to a canonical momentum $p = \hbar k = \hbar q + \hbar G_n$ that differs from the crystal momentum $\hbar q$ by $\hbar G_n$ where G_n is a reciprocal lattice vector. For the 6s-electron surface state of Au the $\hbar G_n$ are orders of magnitude larger than $\hbar q$ and relevant vectors corresponds to a velocity $v = \frac{p}{m} \approx \frac{\hbar G_n}{m} \approx \frac{c}{10}$ that evidently is not concentrated in the non-existent core. It is implied for Au and a magnetic proximity effect, a PMA several orders larger than that predicted by the free electron model [2]. In addition, introduced are electrically controllable spin gaps directly proportional to E , and the periodic potential V , leading to a potential giant PMA. Further discussion of the spin-orbit coupling, along with more details of many of the calculation, is to be found in the Supplementary Materials corresponding to Ref. [22].

Spin Berry phase physics. As explained in any number of texts, see e.g., Ref. [24] the original such phase [25] corresponds to an adiabatic rotation of an applied magnetic field within a time dependent Hamiltonian. However as exemplified by the Stern problem [24] a spin Berry phase can arise for a time independent Hamiltonian simply due to the electron motion within a textured effective magnetic field [3, 26–28]. In Fig. 1a, for the free electron Rashba effect, the spin direction is in-plane and perpendicular to the momentum \vec{p} . When the system is magnetic, as in Fig. 1b, this direction makes a finite angle θ to the direction of a perpendicular magnetisation [2]. Since θ depends upon \vec{p} , even for a uniform magnetisation $\vec{M} = M\hat{\mathbf{z}}$, there is a spin “texture” in momentum space, i.e., an electron sees an internal field that is not parallel to \vec{M} . However for a given momentum \vec{p} , the angle θ is uniform and there is no texture in real space. This is no longer the case when a periodic potential is introduced. In the usual manner, exemplified here in a single dimensional, the spin-up wave-function $\psi_{q_x \uparrow}(x) = \sum_{n_x} e^{-i\theta_{G_{n_x}} s_y / \hbar} u(q_x + G_{n_x}) e^{i(q_x + G_{n_x})x} |\uparrow\rangle$ is written in terms of a crystal moment $\hbar q_x$ and the reciprocal lattice vectors G_{n_x} where n_x is an integer band index and $|\uparrow\rangle$ the spin up ket. The tilt angle $\theta \rightarrow \theta_{G_{n_x}}$ is

4 Giant Rashba electrical control of magnetism in band models

different for different n_x because this is determined by $p_x = \hbar(q_x + G_{n_x})$ and not just $\hbar q_x$. Then, since the phase factor $e^{-i\theta_{G_{n_x}} s_y / \hbar}$ involves s_x , the electron spin direction depends upon the real space position within the unit cell. It is this that introduces a non-trivial spin Berry phase. Just how this works is taken up again below and in the Supplementary Materials[22].

The Kronig-Penney-Nearing model. The Kronig-Penney is a simple model[29] that connects the free electron to the tight binding model. As in Fig. 2a, in a one dimensions, a single atom comprises a square potential well relative to the vacuum. When many atoms are put together, as in

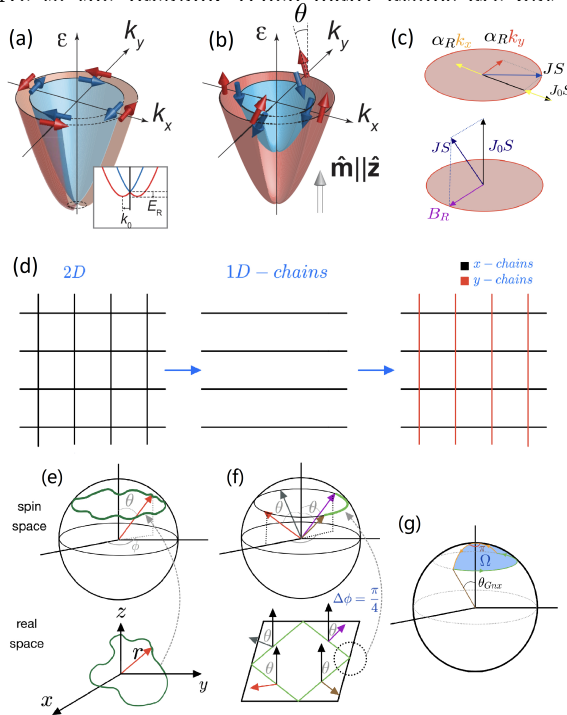


Fig. 1 (a) With a perpendicular electric field $\vec{E} = Ez$ and a given momentum \vec{p} , the Rashba field \vec{B}_R , proportional to $\vec{p} \times \vec{E}$ is tangential to the circles of constant p . (b) In the magnetic case \vec{B}_R has, in addition, a perpendicular component and the axis of quantisation of the spin makes an angle θ to \vec{E} . The angle θ and ϕ determine the Berry phase. (c) Top, with an in-plane magnetisation the Rashba field \vec{B}_R is also in-plane and adds to the exchange field \vec{B}_E . Bottom, the magnetisation and exchange field are perpendicular to the plane while \vec{B}_R is in-plane and adds vectorially to give an effective exchange that makes a momentum dependent angle θ to the perpendicular. (d) Two dimensions corresponds to an array of atoms but can be reduced to a series of crossed chains. (e) A real space path has an image in spin space, i.e., the Bloch sphere. (f) Upon each reflection from perpendicular δ -walls, there is a rotation by $\Delta\phi = \pi/2$ about the z -axis with a constant angle θ . There is a solid angle $\Omega = 2\pi(1 - \cos\theta)$ subtended by this path, leading to a Berry phase $\frac{1}{2}\Omega$ and a finite flux. (g) The up-spin is first rotated by the angle $\theta_{G_{n_x}}$ away the z -axis, then by an angle π about the z -axis and finally back to the z -axis. The closed path subtends a solid angle $\Omega = \pi(1 - \cos\theta_{G_{n_x}})$.

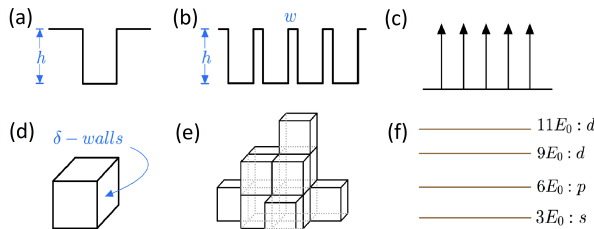


Fig. 2 (a) An atom comprises a region of potential $V(x) = 0$. The surrounding vacuum is at $V(x) = h$. (b) Corresponding to the interstitial region, there is a barrier height h and width w between adjacent the atoms. (c) As $h \rightarrow \infty$ with the product $hw = V$ a constant the interstitials become δ -functions. (d) In three dimensions the atoms are cubes separated by δ -function walls and can be stacked to make a solid as shown in (e). For $V \rightarrow \infty$ the standing waves with $E_{s_x, s_y, s_z} = \frac{\hbar^2}{2m} \left(\frac{\pi}{a}\right)^2 (s_x^2 + s_y^2 + s_z^2)$ have the energy scheme shown in (f). The states with two nodes are split into two non-degenerate triplets with a crystal field splitting $2E_0$.

Fig. 2b, each atom is separated by a barrier corresponding to the interstitial region. If this region is shrunk to zero while at the same time increasing the height of the barrier, the result is a periodic positive delta function potential $V(x) = Va \sum_n \delta(x - na)$ illustrated in Fig. 2c. With decreasing V , individual atomic levels broaden into tight binding bands, then describe nearly free electrons for small V and finally free electrons when $V = 0$. Following Nearing[30] this is generalised to higher dimensions Fig. 2d by assuming a separable potential, e.g., for three dimensions $V(x) + V(y) + V(z)$. Now the atoms correspond to boxes separated by delta function walls and can be stacked as illustrated in Fig. 2e. This model is separable, i.e., the band energy for a crystal wave vector \vec{q} is $E(q_x) + E(q_y) + E(q_z)$ where $E(q_x)$ is a solution to the one dimensional model.

Atoms. Much can be understood from considering three dimensional atoms, i.e., the limit $V \rightarrow \infty$. In the absence spin-orbit coupling, the “atomic” energy levels $E_{n_x, n_y, n_z} = \frac{\hbar^2}{2m} \left(\frac{\pi}{a}\right)^2 (s_x^2 + s_y^2 + s_z^2)$ where the integers s_x , s_y and $s_z = 1, 2, 3, \dots$. Identified is a node-less “s-state” with s_x, s_y and $s_z = 1$. The energy is $3E_0$ where $E_0 = \frac{\hbar^2}{2m} \left(\frac{\pi}{a}\right)^2$ and the band index is $n = 1$. There are three degenerate $E_p = 6E_0$ single node “p-states” $(2, 1, 1)$, $(1, 2, 1)$ and $(1, 1, 2)$. The “d-states”, with two nodes, are crystal field split into two triplets, i.e., $(1, 2, 2)$, $(2, 1, 2)$ and $(2, 2, 1)$ with energy $E_t = 9E_0$ and $(3, 1, 1)$, $(1, 3, 1)$ and $(1, 1, 3)$ with an energy $E_g = 11E_0$. The crystal field splitting is therefore $2E_0$ as shown in the level scheme Fig. 2f. While the $1s$ radial wave-function with no nodes can be identified with $(1, 1, 1)$ the higher non-degenerate ns-states map to the odd $(2n - 1, 2n - 1, 2n - 1)$. All even combinations, e.g. $(2, 2, 2)$ cannot be identified as s-states since they have a node at the centre of the atom. It follows the 6s-orbital of Au, with five radial nodes is properly identified as $(11, 11, 11)$ with energy $363E_0$. Clearly the identification of e.g., higher in energy “p-”, “d-” and “f-” atomic states is an approximate concept given the atomic states here are a representation of the cubic and not rotational group.

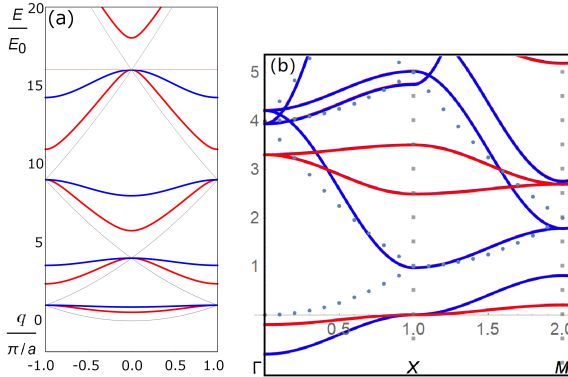


Fig. 3 (a) Free, nearly free ($V = E_0$), and tight binding results ($V = 4E_0$) shown in gray, red and blue. (b) Similar results in two directions for the directions Γ -X-M in first zone.

From free electrons to tight binding As a touchstone for what follows, consider band formation in one and two dimensions. In Fig. 3a the red line correspond to nearly free electrons while the blue line agrees well with the tight binding result[31] $E_{q_x} = E_{n_x} - (-1)^n E_{n_x} \frac{4E_0}{\pi^2 V} \cos q_x a$. Here, and in other figures, the fine grey lines correspond to free electrons. In Fig. 3b are shown bands along high symmetry directions in two dimensions[22].

Stoner magnetism. The problem remains fully separable when the simplest exchange potential $-J_0 \vec{\sigma} \cdot \vec{S}$ is added[32]. Here, \vec{S} is the effective spin, per atom, of the order parameter. As shown in Fig. 4a the minority/majority bands undergo rigid shifts $\pm J_0 S$ relative to those of Fig. 3a.

Spin-orbit coupling As already emphasised, because the atomic potential is flat the full spin-orbit coupling V_{so} simplifies to a Rashba term $\frac{\alpha_R}{\hbar} (\vec{\sigma} \times \vec{p}) \cdot \hat{z}$ in which importantly \vec{p} is the canonical momentum and where $\alpha_R = -\frac{\hbar \lambda_c}{8\pi m c} E$ is proportional to the “applied” and/or intrinsic E fields.

Essential physics in one dimension. The physics behind a PMA, including the effects of the Berry connection \vec{A}_s , can be clearly demonstrated in one dimension. As shown in Fig. 1d the thin film is considered to be a series of chains parallel to the x -direction, with an applied electric field $\vec{E} = E\hat{z}$ in the perpendicular direction. The “perpendicular” case has $\vec{M} = M\hat{z}$ parallel to \vec{E} leading to a Rashba field \vec{B}_R in the y -direction. For the strictly one dimensional model this is degenerate with $\vec{M} = M\hat{x}$. This degeneracy is lifted by adding chains in the y -direction as in Fig. 1c. If the density of electrons on these extra chains is lower, than $\vec{M} = M\hat{x}$ corresponds to an in-plane easy axis. This two chain model is clearly separable, however, the true two dimensional problem is only approximately separable for small α_R [22].

Non-magnetic Rashba effect. The Rashba field $\vec{B}_R = (\alpha_R p_x / \hbar) \hat{y}$ is perpendicular to $\vec{E} = E\hat{z}$ putting the axis of quantisation along the \hat{x} -axis. As indicated in Fig. 4b, the bands are shifted to the left or right by $\Delta q = m\alpha_R / \hbar^2$,

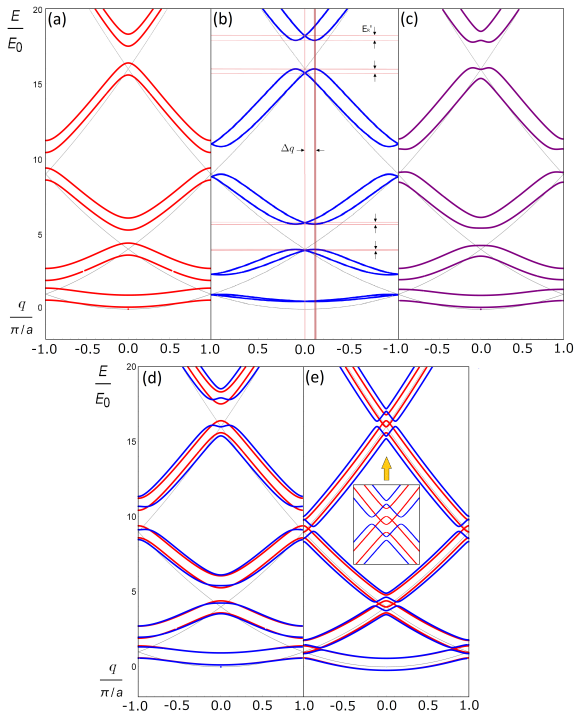


Fig. 4 Lattice Rashba effect. (a) Ferromagnetic case with $V = E_0$ and $J_0S = 0.4E_0$. The bands are shifted up and down by $\pm J_0S$. (b) Non-magnetic Rashba results with $\alpha_R = 0.2 \frac{E_0}{\pi/a}$ showing horizontal shifts by Δq_x . That this shift is independent of the band index n_x is shown by the vertical lines. The horizontal lines illustrated that the empirical value of “ E_R ” depends strongly on n_x . The actual energy shift E_R is however n_x independent. (c) In plane results with $\alpha_R = 0.2 \frac{E_0}{\pi/a}$ and $J_0S = 0.4E_0$. There is a spin-splitting in addition the band shifts. (d) Perpendicular ferromagnetic results. This is similar to (a) but, as can be seen by comparing the red and blue curves, the effective exchange is larger due the vector addition of the Rashba and exchange fields. (e) Similar to (d) but with a smaller crystal potential $V = 0.2E_0$. There are a double gap structures. The first order in E gaps occur away from the high symmetry points ($q = 0$ and $q = \pm \frac{\pi}{a}$). The value of E is doubled between the blue and red curves.

linear in E . That this shift is independent of the band index n_x is illustrated by a vertical line. Also independent of n_x , the energy is lowered by $E_R = \frac{\hbar^2}{2m} \Delta q^2 = \frac{1}{2} m \alpha_R^2 / \hbar^2$. For free electrons E_R can be determined graphically as the vertical distance between the horizontal lines as indicated. This graphical effective “ E_R ” defined in 4b, is correct only for the lowest $n_x = 1$ band, and is almost indiscernible in Fig. 4b. The much larger “ E_R ” reflects the changing band masses. That even the highest band is lowered by only the free electron value $E_R = \frac{1}{2} m \alpha_R^2 / \hbar^2$ is verified by a common horizontal line in Figs. 4b and Fig. 3a, i.e., with and without the Rashba effect. It is implied

the experimental $E_R \approx 3.5\text{meV}$ for Au *cannot* be identified with $\frac{1}{2}m\alpha_R^2/\hbar^2$ and hence used to determine α_R . The real value is much smaller.

In-plane magnetisation. Take $\vec{M} = M\hat{x}$ so that both the exchange $\vec{B}_E = \pm JS_0\hat{y}$ and Rashba $\vec{B}_R = (\alpha_R p_x/\hbar)\hat{y}$ fields are along the y -direction and add to give an apparent exchange $JS = J_0S \pm \alpha_R p_x$. However, e.g., for a majority electron aligned along \vec{M} , the energy $\alpha_R p_x$ can be absorbed into $\frac{\hbar^2}{2m}(p_x - m\alpha_R/\hbar^2)^2 - E_R$ where, as for the non-magnetic case, there is, Fig. 4c, a horizontal shift by $\pm\Delta q_x$ and a band index n_x independent downward energy shift E_R , this in addition to the exchange splitting $\mp J_0S$. Again the evident dependence on the band index n_x arises from the changes in the effective mass. As before, the energy gain is E_R per electron and not the apparent “ E_R ”. The energy shifts are second order in the applied field \vec{E} .

A perpendicular magnetisation. It is important to distinguish between the canonical \vec{p} and crystal momentum $\hbar\vec{q}$. Here $\vec{M} = M\hat{z}$ is parallel to \vec{E} . The Rashba field $\vec{B}_R = (\alpha_R p_x/\hbar)\hat{y}$ is perpendicular to both \vec{M} and \vec{E} . As indicated in the lower part of Fig. 1c, this field adds vectorially to the exchange field $\vec{B}_E = J_0S\hat{z}$. The result is a larger effective exchange $JS = \sqrt{(J_0S)^2 + (\alpha_R/\hbar)^2 p_x^2}$ for an electron of momentum p_x . The axis of quantisation makes an angle $\theta_{p_x} = \tan^{-1}[(\alpha_R p_x/\hbar)/(J_0S)]$ to the direction of \vec{M} . In Fig. 4d, in red, is reproduced Fig. 4a while in blue is the result including the Rashba effect. Except near the points where the free electron bands cross, the results are well reproduced by the analytic tight binding solution[22], $E_{n_x}^{\pm}(q) = E_{n_x} - \frac{4E_0 E_{n_x}}{V} \cos qa \mp \left(J_0S + \alpha_R^2 \frac{\hbar^4}{8J_0S} G_{n_x}^2 \right)$. The effective exchange splitting for the blue curve is indeed manifestly larger than that of the red curves.

The Rashba effect increases dramatically for higher energy bands reflecting the increase in the reciprocal lattice vectors G_{n_x} for larger band index n_x . This is one of the principal results and is a consequence of that fact that the Rashba effect for the full V_{so} involves the canonical $\hbar p_x$ and not just the crystal momentum $\hbar q_x$.

For the surface state of Au $q_F \approx \frac{1}{10} \frac{2\pi}{a} \approx 1.5\text{\AA}^{-1}$. The Rashba field is $B_F = \alpha_R q_F \approx \alpha_R \frac{1}{10} \frac{2\pi}{a}$ for the $n_x = 1$ “s-band”. In contrast the $n_x = 3$ “d-band”, with the same crystal momentum, has a Rashba field proportional to $\frac{2\pi}{10a} + 3\frac{2\pi}{a} \approx 3\frac{2\pi}{a}$. The splitting in Fig. 4d is proportional to B_R^2 and almost 10^3 times larger. This should be compared with the discussion of Fig. 4c corresponding to an in-plane magnetisation. In that case the energy gain was E_R per electron independent of the band index n_x . As a consequence for magnetic thin films the Rashba spin-orbit splitting leads to unambiguously to a PMA. The near cancellation for two dimensions noted in [2] no longer occurs. The Rashba field in Tesla is estimated using $B_R = \frac{v}{2c} \frac{E}{c}$. The Au-Au separation is $\approx 2.84\text{\AA}$, but the interstitial region that has been shrunk to zero and the model does not localise the electrons as strongly as does a central potential. Using half this distance gives $v \approx \frac{c}{5}$ and $B_R \approx \frac{E}{10c}$. For Au the experimental $B_R \approx 5 \times 10^2\text{T}$ corresponding to an internal field of $E \sim 10^{12}\text{V/m}$. The break down field of

a good gate oxide, e.g. Al_2O_3 is $E \sim 10^9 \text{V/m}$ and sets the scale, although the local electrical field can easily be 10^{10}V/m corresponding to $B_R \sim 3\text{T}$. In order to realise a PMA field of this magnitude needed is a small proximity exchange field such that $B_E = J_0 S \approx B_R$.

Electrically controllable gaps. The effects of the Berry phase physics are evident in Fig. 4d. The tight binding result is clearly inadequate in the region near the crossing of the free electron bands. There is no longer a simple increase in the effective exchange and the results (blue) with the Rashba effect cross those (red) for which this is absent. The origin of this effect is evident from the insert in Fig. 4e. In the absence of the Rashba coupling, there are crossings, either side of $q_x = 0$, of red pair of curves with the upper and lower lines corresponding to majority/minority bands. Reflecting the Berry phase factor $e^{-i\theta_{G_{n_x}} s_x / \hbar}$ in $\psi_{q_x \uparrow}(x)$ there are matrix elements proportional to $\sin \theta_{G_{n_x}} \sim \frac{\alpha_R G_{n_x}}{J_0 S}$ that connect the majority/minority bands when an electron scatters off the periodic potential $V(x)$. This produces gaps[22] that go as $V \theta_{G_{n_x}} \sim V \frac{\alpha_R G_{n_x}}{J_0 S}$ and since α_R is proportional to the electric field E , so are these gaps. While in Fig. 4e there are two distinct gaps at the majority/minority crossing, with an increasing periodic potential V these gaps broaden and merge as in Fig. 4d. Reflecting the dependence on G_{n_x} , there is a very strong increase in these gaps with increasing energy and band index n_x . In Figs. 4d and Fig. 4e, the Berry phase gap goes from being barely visible for $E \sim 2E_0$ and $q_x \lesssim \frac{\pi}{a}$, to being comparable to that due to the periodic potential at $E \sim 4E_0$ and $q_x \approx 0$, and larger than the periodic gap for $E \sim 9E_0$ and $q_x \lesssim \frac{\pi}{a}$. That for higher energies the gap hardly increases, e.g., from $E \sim 9E_0$ to $16E_0$ reflects the fact that the Rashba energy $\alpha_R G_{n_x=3}$ is comparable to $J_0 S$, the exchange splitting. Again these changes are due to the fact that the Rashba effect reflects the full momentum $p_x = \hbar(q_x + G_{n_x})$ and not just the crystal momentum $\hbar q_x$. For a magnetic proximity effect engineered to have $J_0 S \approx \alpha_R G_{n_x}$ ($B_E \approx B_R$) the effective field is $\sim V$ in energy units and easily of the order of electron volts. In the illustrative calculations, of this and previous sections, the value of α_R is unrealistically large and chosen to make evident the various effects.

Peierls effect. These electrically controlled gaps occur at critical values of the wave-vector $\vec{q} = \vec{q}_c$ at which occurs an accidental crossing of minority/-majority bands. That such gaps lie at the Fermi energy E_F and produce a PMA linear in E is therefore very much material dependent. However a Peierls effect can occur in which \vec{M} tilts an angle α away from the vertical thereby creating a shift Δq , proportional to the in-plane component of \vec{M} , that moves \vec{q}_c to the Fermi surface. In this manner there is not only an electrical control of the PMA but also of the tilt angle. Since the spin torque transfer (STT) effect[3, 6] is absent, and highly dissipative, for a strictly perpendicular \vec{M} , this is of considerable technological importance.

Mathematical methods. Schrödinger's equation reduces to[22]:

$$\frac{1}{V} = \sum_{n_x} \mathcal{G}_{n_x}(E_{q_x}) \quad (1)$$

where V is the strength of the delta function potentials. This is written in terms of the free electron Green's function, e.g., with a perpendicular magnetisation $\mathcal{G}_n(E_{q_x}) = e^{-i\theta_{G_{n_x}} s_x / \hbar} (E_{q_x} - \frac{\hbar^2 (q_x + G_{n_x})^2}{2m} - \sigma_z JS)^{-1} e^{i\theta_{G_{n_x}} s_x / \hbar}$, a two-by-two matrix. Exploiting the SU(2) algebra, Eq. 1 reduces to the form $\frac{1}{V} = \mathcal{S} + \mathcal{A}\sigma_z + \mathcal{B}\sigma_y$ and finally to an implicit secular equation for E_{q_x} : $(\frac{1}{V} - \mathcal{S})^2 - (\mathcal{A}^2 + \mathcal{B}^2) = 0$ with rather complicated definitions of the three functions \mathcal{S} , \mathcal{A} and \mathcal{B} , see[22]. This non-linear equation has many solutions for a given q_x . These are found using Mathematica and are assigned a band index n_x by comparison with the atomic limit.

Approximate separation of variables in two dimensions. Since the spin orbit terms $\frac{\alpha_R}{\hbar} \sigma_x p_y$ and $-\frac{\alpha_R}{\hbar} \sigma_y p_x$ act on the same spin ket $|\rangle$ an exact separation is not possible. This notwithstanding[22] if the Rashba field B_R is small compared with exchange field B_E , defined is separation *matrix*, e.g., $M_x = \frac{1}{\psi_x(x)} \hat{H}_x \psi_x(x)$ containing three independent constants obtained by requiring \mathcal{S} , \mathcal{A} and \mathcal{B} all to be zero. The matrix M_y is similarly defined and finally $[(M_x + M_y) - E]|\rangle = 0$, where E is the energy, is solved for the spin ket $|\rangle$. Except for the gaps, the essentially physics is contained in the two dimensional tight binding results. The net PMA energy $\alpha_R^2 \frac{\hbar^4}{8J_0S} G_{n_y}^2 - \frac{\hbar^2 m^2}{2m \hbar^4} \alpha_R^2 E^2$ is dominated by the term proportional to the $G_{n_y}^2$. There is a ‘‘enormous’’ E^2 perpendicular anisotropy energy PMA as reported e.g., by Lau et al [33].

A different Berry phase. The introduction of a Berry phase has become quite popular. The Berry phase physics introduced here is different. In particular the Berry connection \vec{A}_s , i.e., an effective vector potential defined elsewhere[3] contains an off-diagonal part that is invariably ignored. It is this part of \vec{A}_s that leads to the electrically controlled gaps described above. This is taken up again immediately below.

The spin-orbit coupling implies a Luttinger anomalous velocity[34] and this leads to Berry phase corrections to the dynamical equations of motion. As described by Yao et al.[13] these dynamics can be scotched onto a relativistic band calculation. Invariably the band structure package, in this case WIEN2K[15], includes only the effects of a central potential. In another approach[26–28] a spin Berry phase reflects a spin texture, i.e., non-co-linear magnetisation $\vec{M}(\vec{r}; t)$. In the present development the central potential $V(r)$ is absent and the order parameter $\vec{M}(\vec{r}; t)$ is uniform. Again, this new Berry phase physics cannot be captured in the current flavours of the DFT[16–19, 35].

Berry phase physics - perpendicular magnetisation. In this case, Eq. 1 becomes

$$\frac{1}{V} = \sum_{n_x, \pm} (1 \pm e^{-i\frac{\pi}{2}(\cos\theta_{G_{n_x}} + \sigma_z)\sigma_z + \sin\theta_{G_{n_x}}\sigma_y}) \mathcal{G}_{G_{n_x}}^{\pm} \quad (2)$$

where $\mathcal{G}_{n_x}^{\pm} = [E_{q_x} - \frac{\hbar^2 (q_x + G_{n_x})^2}{2m} \pm JS]^{-1}$ exhibits the exchange splitting JS including the Rashba correction[22] and corresponds to the dynamic phase. The phase factor $e^{-i\frac{\pi}{2}(\cos\theta_{G_{n_x}} + \sigma_z)\sigma_z + \sin\theta_{G_{n_x}}\sigma_y}$ is that generated[22] by the Berry connection[3] \vec{A}_s for the spin path shown in Fig. 1g that involves a ϕ rotation of π at an angle $\theta_{G_{n_x}}$. Consider a more intuitive two dimensional

example. As shown in Fig. 1e, a real space path of an electron maps to one on the Bloch sphere. In Fig. 1f, an electron executes a closed path by undergoing elastic reflections with four crystal planes. The spin always makes the same angle θ to the direction of $\vec{E} = E\hat{z}$ but, since the momentum has a different direction, the angle ϕ changes by $\frac{\pi}{2}$ at each reflection. There is a solid angle Ω subtended by the path on the Bloch sphere leading to a diagonal Berry phase $\frac{1}{2}\Omega$.

Advancing to the Iron Age. The Lieb proof[36] of the Hohenberg-Kohn theorem[37] and the resulting Kohn-Sham equations[38] do not admit a non-trivial Berry connection \vec{A}_s . The constrained diamagnetic DFT[39] *does* admit an electromagnetic Berry connection \vec{A} as an *extrinsic* potential[40] and hence admits a magnetic field. For a fraction $\frac{p}{q}$ of the flux quantum per unit cell, a Hofstadter butterfly[41] occurs in which the unit cell is q times larger. Even this possibility is not included in current flavours of the DFT. Worse, the spin Berry connection \vec{A}_s introduced here[3] is *intrinsic* whence this extension is not valid. In Greek mythology the Golden Age leads finally to the Iron Age. It might be hoped the much heralded materials golden age based on the DFT[42] will soon describe the essential Berry phase physics of capped iron thin-films with a Rashba PMA.

Summary. When compared with the free electron model[2], accounting for the periodic potential leads an enormous Rashba PMA proportional to E^2 . Illustrating the importance of the usually ignored off-diagonal part of the spin Berry connection[3] \vec{A}_s , found are electrically controlled band structure gaps proportional to E with the promise of a truly giant, linear in E , electrical control of magnetism accompanied by a spin Peierls effect that implies low dissipation dynamics.

References

- [1] L. Wang, X. Li, T. Sasaki, K. Wong, G. Yu, S. Peng, C. Zhao, T. Ohkubo, K. Hono, W. Zhao, K. Wang, High voltage-controlled magnetic anisotropy and interface magnetoelectric effect in sputtered multilayers annealed at high temperatures. *Science China Physics, Mechanics & Astronomy* **63**(7), 277,512 (2020). <https://doi.org/10.1007/s11433-019-1524-y>. URL <https://doi.org/10.1007/s11433-019-1524-y>
- [2] S.E. Barnes, J. Ieda, S. Maekawa, Rashba spin-orbit anisotropy and the electric field control of magnetism. *Scientific Reports* **4**(1), 4105 (2014). <https://doi.org/10.1038/srep04105>. URL <https://doi.org/10.1038/srep04105>
- [3] S.E. Barnes, in *Spin Current*, ed. by S. Maekawa, S.O. Valenzuela, E. Saitoh, T. Kimura (Oxford Scholarship, 2013), chap. 7
- [4] G. Grüner, The dynamics of charge-density waves. *Rev. Mod. Phys.* **60**, 1129–1181 (1988). <https://doi.org/10.1103/RevModPhys.60.1129>. URL <https://doi.org/10.1103/RevModPhys.60.1129>

<https://link.aps.org/doi/10.1103/RevModPhys.60.1129>

- [5] S.E. Barnes, A. Zawadowski, Theory of josephson-type oscillations in a moving charge-density wave. *Phys. Rev. Lett.* **51**, 1003–1006 (1983). <https://doi.org/10.1103/PhysRevLett.51.1003>. URL <https://link.aps.org/doi/10.1103/PhysRevLett.51.1003>
- [6] J. Slonczewski, Current-driven excitation of magnetic multilayers. *Journal of Magnetism and Magnetic Materials* **159**(1), L1–L7 (1996). [https://doi.org/https://doi.org/10.1016/0304-8853\(96\)00062-5](https://doi.org/https://doi.org/10.1016/0304-8853(96)00062-5). URL <https://www.sciencedirect.com/science/article/pii/0304885396000625>
- [7] A. Messiah, *Quantum Mechanics* (Dover Publications, 2014)
- [8] L.L. Foldy, S.A. Wouthuysen, On the dirac theory of spin 1/2 particles and its non-relativistic limit. *Phys. Rev.* **78**, 29–36 (1950). <https://doi.org/10.1103/PhysRev.78.29>. URL <https://link.aps.org/doi/10.1103/PhysRev.78.29>
- [9] R. Winkler, *Spin-orbit coupling effects in two-dimensional electron and Hole Systems* (Springer, 2011)
- [10] X. Wang, R. Wu, D.S. Wang, A.J. Freeman, Torque method for the theoretical determination of magnetocrystalline anisotropy. *Phys. Rev. B* **54**, 61–64 (1996). <https://doi.org/10.1103/PhysRevB.54.61>. URL <https://link.aps.org/doi/10.1103/PhysRevB.54.61>
- [11] Y.A. Bychkov, É.I. Rashba, Properties of a 2D electron gas with lifted spectral degeneracy. *Soviet Journal of Experimental and Theoretical Physics Letters* **39**, 78 (1984)
- [12] P.V. Ong, N. Kioussis, D. Odkhuu, P. Khalili Amiri, K.L. Wang, G.P. Carman, Giant voltage modulation of magnetic anisotropy in strained heavy metal/magnet/insulator heterostructures. *Phys. Rev. B* **92**, 020,407 (2015). <https://doi.org/10.1103/PhysRevB.92.020407>. URL <https://link.aps.org/doi/10.1103/PhysRevB.92.020407>
- [13] Y. Yao, L. Kleinman, A.H. MacDonald, J. Sinova, T. Jungwirth, D.S. Wang, E. Wang, Q. Niu, First principles calculation of anomalous hall conductivity in ferromagnetic bcc Fe. *Phys. Rev. Lett.* **92**, 037,204 (2004). <https://doi.org/10.1103/PhysRevLett.92.037204>. URL <https://link.aps.org/doi/10.1103/PhysRevLett.92.037204>
- [14] A. Manchon, H.C. Koo, J. Nitta, S.M. Frolov, R.A. Duine, New perspectives for Rashba spin–orbit coupling. *Nature Materials* **14**(9), 871–882 (2015). <https://doi.org/10.1038/nmat4360>. URL <https://doi.org/10.1038/nmat4360>

- [15] P. Blaha, K. Schwarz, G. Madsen, D. Kvasnicka, J. Luitz, R. Laskowski, F. Tran, L. Marks, L. Marks, *WIEN2k: An Augmented Plane Wave Plus Local Orbitals Program for Calculating Crystal Properties* (Techn. Universitat, 2019)
- [16] D. Hobbs, G. Kresse, J. Hafner, Fully unconstrained noncollinear magnetism within the projector augmented-wave method. *Phys. Rev. B* **62**, 11,556–11,570 (2000). <https://doi.org/10.1103/PhysRevB.62.11556>. URL <https://link.aps.org/doi/10.1103/PhysRevB.62.11556>
- [17] G. Kresse, J. Furthmüller, Efficient iterative schemes for ab initio total-energy calculations using a plane-wave basis set. *Phys. Rev. B* **54**, 11,169–11,186 (1996). <https://doi.org/10.1103/PhysRevB.54.11169>. URL <https://link.aps.org/doi/10.1103/PhysRevB.54.11169>
- [18] G. Kresse, J. Furthmüller, Efficiency of ab-initio total energy calculations for metals and semiconductors using a plane-wave basis set. *Computational Materials Science* **6**(1), 15–50 (1996). [https://doi.org/https://doi.org/10.1016/0927-0256\(96\)00008-0](https://doi.org/https://doi.org/10.1016/0927-0256(96)00008-0). URL <https://www.sciencedirect.com/science/article/pii/0927025696000080>
- [19] D. Hobbs, G. Kresse, J. Hafner, Fully unconstrained noncollinear magnetism within the projector augmented-wave method. *Phys. Rev. B* **62**, 11,556–11,570 (2000). <https://doi.org/10.1103/PhysRevB.62.11556>. URL <https://link.aps.org/doi/10.1103/PhysRevB.62.11556>
- [20] S. Koseki, N. Matsunaga, T. Asada, M.W. Schmidt, M.S. Gordon, Spin-orbit coupling constants in atoms and ions of transition elements: Comparison of effective core potentials, model core potentials, and all-electron methods. *The Journal of Physical Chemistry A* **123**(12), 2325–2339 (2019). <https://doi.org/10.1021/acs.jpca.8b09218>. URL <https://doi.org/10.1021/acs.jpca.8b09218>. PMID: 30817150. <https://arxiv.org/abs/https://doi.org/10.1021/acs.jpca.8b09218>
- [21] L D Landau, E.M. Lifshitz *Quantum mechanics: non-relativistic theory* (Butterworth Heinemann, 1991)
- [22] See the supplementary materials for details of the calculations.
- [23] The integral $\langle \frac{1}{r^3} \rangle = \frac{Z^3}{n^3 \ell(\ell+\frac{1}{2})(\ell+1)} \frac{1}{a_0^3}$, so if $\ell = 1$ then $n = 2$ and there is an additional factor of $\frac{1}{n^3 \ell(\ell+\frac{1}{2})(\ell+1)} = \frac{1}{24}$. For the estimation of the electric field $\langle \frac{1}{r^2} \rangle = \frac{2Z^2}{n^3(2\ell+1)a_0^2}$ is used
- [24] R. Shankar, *Principles of Quantum Mechanics* (Springer, 2014)

- [25] M.V. Berry, Quantal Phase Factors Accompanying Adiabatic Changes. Proceedings of the Royal Society of London Series A **392**(1802), 45–57 (1984). <https://doi.org/10.1098/rspa.1984.0023>
- [26] J. Ye, Y.B. Kim, A.J. Millis, B.I. Shraiman, P. Majumdar, Z. Tešanović, Berry phase theory of the anomalous Hall effect: Application to colossal magnetoresistance manganites. Phys. Rev. Lett. **83**, 3737–3740 (1999). <https://doi.org/10.1103/PhysRevLett.83.3737>. URL <https://link.aps.org/doi/10.1103/PhysRevLett.83.3737>
- [27] Y. Taguchi, Y. Oohara, H. Yoshizawa, N. Nagaosa, Y. Tokura, Spin chirality, Berry phase, and anomalous Hall effect in a frustrated ferromagnet. Science **291**, 2573–2576 (2001). <https://doi.org/10.1126/science.1058161>
- [28] R. Shindou, N. Nagaosa, Orbital ferromagnetism and anomalous Hall effect in antiferromagnets on the distorted fcc lattice. Phys. Rev. Lett. **87**, 116,801 (2001). <https://doi.org/10.1103/PhysRevLett.87.116801>. URL <https://link.aps.org/doi/10.1103/PhysRevLett.87.116801>
- [29] R.D.L. Kronig, W.G. Penney, R.H. Fowler, Quantum mechanics of electrons in crystal lattices. Proceedings of the Royal Society of London. Series A, Containing Papers of a Mathematical and Physical Character **130**(814), 499–513 (1931). <https://doi.org/10.1098/rspa.1931.0019>. URL <https://royalsocietypublishing.org/doi/abs/10.1098/rspa.1931.0019>. <https://arxiv.org/abs/https://royalsocietypublishing.org/doi/pdf/10.1098/rspa.1931.0019>
- [30] James Nearing. Unpublished
- [31] V. Rosato, M. Guillope, B. Legrand. Thermodynamical and structural properties of f.c.c. transition metals using a simple tight-binding model (1989). <https://doi.org/10.1080/01418618908205062>. URL <https://www.tandfonline.com/doi/abs/10.1080/01418618908205062>
- [32] E.C. Stoner, E.P. Wohlfarth, A mechanism of magnetic hysteresis in heterogeneous alloys. Philosophical Transactions of the Royal Society of London. Series A, Mathematical and Physical Sciences **240**(826), 599–642 (1948). <https://doi.org/10.1098/rsta.1948.0007>. URL <https://royalsocietypublishing.org/doi/abs/10.1098/rsta.1948.0007>. <https://arxiv.org/abs/https://royalsocietypublishing.org/doi/pdf/10.1098/rsta.1948.0007>
- [33] Y.C. Lau, Z. Chi, T. Taniguchi, M. Kawaguchi, G. Shibata, N. Kawamura, M. Suzuki, S. Fukami, A. Fujimori, H. Ohno, M. Hayashi, Giant perpendicular magnetic anisotropy in Ir/Co/Pt multilayers. Phys. Rev. Materials **3**, 104,419 (2019). <https://doi.org/10.1103/PhysRevMaterials.3.104419>. URL <https://link.aps.org/doi/10.1103/PhysRevMaterials.3.104419>

- [34] R. Karplus, J.M. Luttinger, Hall effect in ferromagnetics. *Phys. Rev.* **95**, 1154–1160 (1954). <https://doi.org/10.1103/PhysRev.95.1154>. URL <https://link.aps.org/doi/10.1103/PhysRev.95.1154>
- [35] G. Chaudhary, M.d.S. Dias, A.H. MacDonald, S. Lounis, Anatomy of magnetic anisotropy induced by Rashba spin-orbit interactions. *Phys. Rev. B* **98**, 134,404 (2018). <https://doi.org/10.1103/PhysRevB.98.134404>. URL <https://link.aps.org/doi/10.1103/PhysRevB.98.134404>
- [36] E.H. Lieb, Density functionals for coulomb systems. *International Journal of Quantum Chemistry* **24**(3), 243–277 (1983). <https://doi.org/https://doi.org/10.1002/qua.560240302>. URL <https://onlinelibrary.wiley.com/doi/abs/10.1002/qua.560240302>. <https://arxiv.org/abs/https://onlinelibrary.wiley.com/doi/pdf/10.1002/qua.560240302>
- [37] P. Hohenberg, W. Kohn, Inhomogeneous electron gas. *Phys. Rev.* **136**, B864–B871 (1964). <https://doi.org/10.1103/PhysRev.136.B864>. URL <https://link.aps.org/doi/10.1103/PhysRev.136.B864>
- [38] W. Kohn, L.J. Sham, Self-consistent equations including exchange and correlation effects. *Phys. Rev.* **140**, A1133–A1138 (1965). <https://doi.org/10.1103/PhysRev.140.A1133>. URL <https://link.aps.org/doi/10.1103/PhysRev.140.A1133>
- [39] W. Kohn, A. Savin, C.A. Ullrich, Hohenberg–Kohn theory including spin magnetism and magnetic fields. *International Journal of Quantum Chemistry* **101**(5), 20–21 (2005). <https://doi.org/https://doi.org/10.1002/qua.20303>. URL <https://onlinelibrary.wiley.com/doi/abs/10.1002/qua.20303>. <https://arxiv.org/abs/https://onlinelibrary.wiley.com/doi/pdf/10.1002/qua.20303>
- [40] G. Vignale, M. Rasolt, Current- and spin-density-functional theory for inhomogeneous electronic systems in strong magnetic fields. *Phys. Rev. B* **37**, 10,685–10,696 (1988). <https://doi.org/10.1103/PhysRevB.37.10685>. URL <https://link.aps.org/doi/10.1103/PhysRevB.37.10685>
- [41] S. Janecek, M. Aichinger, E.R. Hernández, Two-dimensional Bloch electrons in perpendicular magnetic fields: An exact calculation of the Hofstadter butterfly spectrum. *Phys. Rev. B* **87**, 235,429 (2013). <https://doi.org/10.1103/PhysRevB.87.235429>. URL <https://link.aps.org/doi/10.1103/PhysRevB.87.235429>
- [42] R. Adler, C.J. Kang, C.H. Yee, G. Kotliar, Correlated materials design: prospects and challenges. *Reports on Progress in Physics* **82**(1), 012,504 (2018). <https://doi.org/10.1088/1361-6633/aadca4>. URL <https://doi.org/10.1088%2F1361-6633%2Faadca4>